Materials & Design 239 (2024) 112792

Contents lists available at ScienceDirect

Materials & Design

journal homepage: www.elsevier.com/locate/matdes

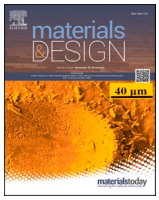

Terrene 2.0: Biomaterial composites design & shellular structures development for augmented earthen construction

Liam Lasting [a], Mostafa Akbari [b], Destynn Keuchel [a], Na Kyung Lee [a], Shravan Pradeep [d,e], Shivani Chawla [a], Abigail Weinstein [a], Masoud Akbarzadeh [b,c], Laia Mogas-Soldevila [a,*]

[a] DumoLab Research, Weitzman School of Design, University of Pennsylvania, Philadelphia, PA, USA
[b] Polyhedral Structures Laboratory, Weitzman School of Design, University of Pennsylvania, Philadelphia, PA, USA
[c] General Robotic, Automation, Sensing and Perception (GRASP) Lab, School of Engineering, University of Pennsylvania, Philadelphia, PA, USA
[d] Complex Fluids Lab, Department of Mechanical Engineering and Applied Mechanics, University of Pennsylvania, Philadelphia, PA, USA
[e] Penn Soft Earth Dynamics Lab, Department of Earth and Environmental Science, University of Pennsylvania, Philadelphia, PA, USA

ARTICLE INFO

Keywords:
Sustainable Material Composites
Sand-based Materials
Multiscale Material Behavior
Reusable Formwork
Polyhedral Graphic Statics
Anticlastic Shellular Structures

ABSTRACT

To transition the construction industry towards sustainable practices, we challenge wasteful methods and non-renewable systems by harnessing local biological materials and augmenting them to describe contemporary forms. Our work enhances the primarily compressive material properties of sand-based compounds to develop a construction method for tension–compression anticlastic shellular structures. We have developed a novel bilayer system with multiscale induced behavior called ChitoSand, made primarily of a sand matrix, incorporating chitosan biopolymer as a microstructural binder, short flax fibers to boost tensile capacity at the mesoscale, and citric acid to increase plasticity, which is then underlaid by a sewn burlap fabric base layer to raise the bending capacity at the macroscale. This produces a fully biodegradable material system that we paired with anticlastic geometry calculations to enhance effective material use and structural form. We then developed an earthen construction workflow that uses reusable pneumatic formwork holding the ChitoSand bilayer composite during hardening in ambient conditions. This research yields a tension–compression system with modern geometry and a minimized environmental footprint.

1. Introduction: Towards augmented earthen construction

With a global human population of eight billion people, projections indicate that more buildings will be constructed in the next 50 years than in the past 2,000 [1]. This remarkable expansion comes amidst heightened concerns for the environment and the significant carbon dioxide (CO_2) emissions attributed to the construction industry, responsible for approximately 40 % of global energy-related CO_2 emissions [2,3] and for one-third of global solid waste [4]. A re-evaluation of industry standards and a quest for alternatives to conventional construction materials and methods is imperative. While ecological integration in architectural design is rising, fundamental flaws lie in typical long-distance material sourcing, assembled into non-recyclable construction details, with widespread use of concrete-based structures causing 8 % of CO_2 of the abovementioned emissions. In recent years, new construction methods have emerged for minimal waste production, and, while still limited in scale and location, researchers are exploring potentially eliminating the need for formwork altogether in the construction of complex geometric forms [5,1,6] by, for instance, using large-scale 3D-printed technologies to develop full habitats [7]. While complete formwork elimination is one approach, there are also sustainable alternatives that employ reusable formwork [8]. In 1942, Wallace Neff pioneered the use of pneumatic formwork, giving rise to concrete domes known as bubble homes [9]. Though these forms primarily consisted of compression-only concrete shells that limited geometric possibilities, they provided affordable and suitable dwellings. The method has since progressed to produce more complex geometries [10], such as a double-curved anticlastic pavilion that employs stretched computationally knit fabric coated by a thin concrete shell and utilizes external wooden frames to temporarily tension the fabric until the concrete sets [11]. This project illustrates the potential to reduce waste during construction while enabling geometrically intricate forms.

Beyond altering formwork methods, material compositions and manufacturing processes require reevaluation towards biobased

* Corresponding Author at: 210 S 34th St, Meyerson Hall #207B, Philadelphia, PA 19104, USA.
E-mail address: laiams@design.upenn.edu (L. Mogas-Soldevila).

https://doi.org/10.1016/j.matdes.2024.112792
Received 20 July 2023; Received in revised form 28 January 2024; Accepted 22 February 2024
Available online 1 March 2024

alternatives. The globalization of the construction industry and the pervasive adoption of the international style have led to a heavy reliance on non-local materials that undergo environmentally taxing manufacturing processes [12]. The production of glass, concrete, and steel contributes to approximately one-quarter of the construction industry's CO_2 emissions [3]. A shift is emerging in modern architectures incorporating new fabrication methods and advocacy for temporality over permanence is growing with sustainable, material-driven design as the starting point and outputting innovative systems such as additive manufactured raw earth domes [13], biopolymer skins from shrimp shells [14], mycelium brick towers that compost into fertilizer [15], coconut agricultural by-products pressed into cladding panels [16], algae and wood frame shells reviving vernacular plastic-free times [17]. These materials and methods do not rely on the extraction of finite resources but rather on the integration of sustainable and renewable resources that promote the health and biodiversity of the surrounding environment [18].

Valuable insights can be gleaned from vernacular structures. Earthen structures have been built for centuries, composed of soils and clays that dry into bricks and walls, and are still prevalent in many regions worldwide [19,20]. Once these structures have served their purpose and are no longer maintained, they naturally return to their original state. In contrast, once the curing process of concrete begins, its physical state becomes irreversible, hindering the material's recyclability [21,22]. While earthen structures may not possess the same strength and stability as concrete, the introduction of renewable additives into the soil mix can enhance its mechanical properties. In nature, most materials are composites of primarily polymeric and ceramic substances. For instance, bone, shell, and coral are made of hydroxyapatite, calcite, or aragonite bound within a matrix of collagen and are tougher than engineered ceramics with comparable tensile strength [12]. Combining this knowledge with ancient earthen construction practices, natural additives, and biotechnology, new research is developing material blends and construction methods producing hemp and lime walls [23], reinforced rammed earth blocks with sand and barley fibers [24], regolith and chitosan hydrogel solids for martian habitats [25], natural fiber-reinforced cement and concrete formulations aiming to replace high-carbon-footprint steel and fiberglass fibers with carbon fixing ones such as banana and coconut [27], or living building materials such as bacterial biomineralized hydrogel-sand composites able to self-heal [28] or microorganism grown biocements [29].

Our work contributes to the transition of the construction industry towards material-driven, sustainable practices. We challenge wasteful methods and non-renewable systems by harnessing local biological materials and enhancing them to describe contemporary forms. Terrene 2.0 merges optimized structural design methods (Fig. 1a–b) with biomaterial compounds (Fig. 1e–h) to develop a construction method for tension–compression anticlastic shellular structures (Fig. 1c–d) and enhance the primarily compressive material properties of sand.

2. Materials and methods

2.1. ChitoSand materials

A novel ChitoSand biomaterial is composed of 92.4 % w/w sand, 1.45 % w/w chitosan biobinder, 0.84 % w/w flax fiber, 1.73 % w/w citric acid, and 3.56 % w/w burlap underlayer + chitosan hardener. Quikrete's all-purpose sand with a granularity of 1–2 mm was purchased from Home Depot; VintageLineStyle's natural flax fiber 1–5 cm was purchased from Etsy; Burlap fabric and PVC-coated polyester fabric were purchased from Fleishman Fabrics and sewn together using a Singer MX231 sewing machine with Coats & Clark Dual Duty XP Heavy Thread. The pneumatic structure was sealed using the Gorilla Waterproof Caulk & Seal 100 % Silicone Sealant. High molecular weight Chitosan at 85 % deacetylation was purchased from TidalVision and processed at 7 % w/v in 4 % w/v acetic acid in an aqueous solution and used as a binder in the ChitoSand mixture and to impregnate burlap fabric. The Terrene 2.0 mixtures components were measured using a SurmountWay high-precision digital laboratory scale with a 10 kg x 0.1 g accuracy.

2.2. Mechanical Characterization

Compressive Strength Testing of ChitoSand Top Layer:

Twelve samples of ChitoSand without flax fiber are cast in laser cut acrylic cylindrical molds with a diameter of 13 mm and a height of 6 mm. After drying at an ambient temperature in the mold for 66 h, these specimens are tested with an Instron 4206 UTM (Universal Testing Machine) with a uniaxial loading rate of 1 mm/min with a 12.5 kN load cell. Twelve samples of ChitoSand compound (including flax fiber) are cast in a 32 mm3 cube silicone mold. These samples are dried in a ColeParmer incubator oven at 50 °C for 24 h in the mold and in ambient conditions for another 24 h. An Instron 4206 UTM is used for the compression test with a loading rate of 2 mm/min with a 25 kN load cell 2b-c).

3-Point Bend Testing of ChitoSand Top Layer: Ten 211x26x11 mm samples of ChitoSand [30] are prepared in accordance with the ASTM D790 Flexural Test Procedure A (Standard Test Methods for Flexural Properties of Unreinforced and Reinforced Plastics and Electrical Insulating Materials). Molds are made from acrylic bars fixed with clamps for effective release of the sample. The samples are desiccated in a ColeParmer incubator at 50 °C for 24 h with the mold and 24 h in ambient conditions. An Instron 5564 Tabletop UTM is used for the 3-point bending test with a support span of 176 mm and at a loading rate of

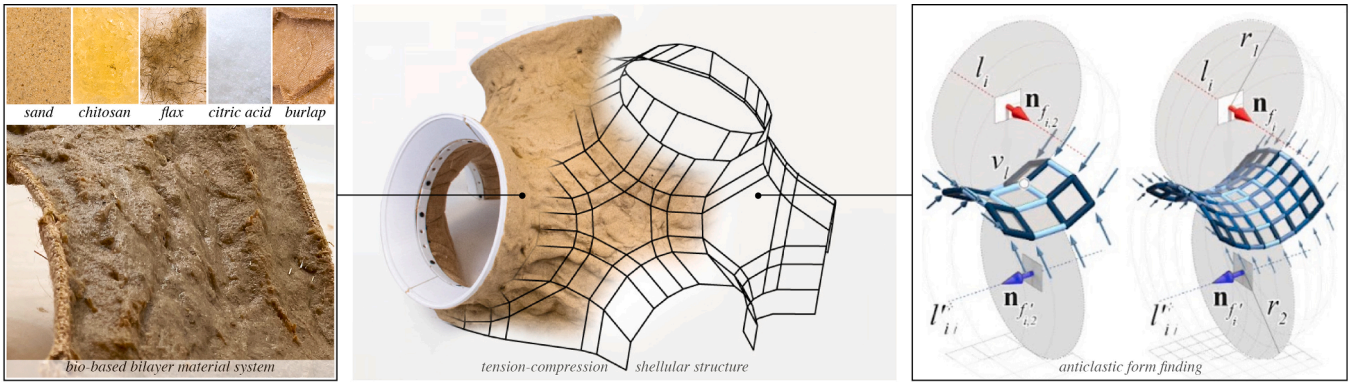

Fig. 1. Terrene 2.0 Summary Diagram. Structural Design and Construction Method including; (A) form's polyhedral force diagram, (B) 'hybrid' geometry, (C) pneumatic formwork, (D) burlap sleeve. ChitoSand Bilayer Material Design including; (E) sand base, (F) short natural fibers, (G) natural plasticizer, (H) hydrogel binder.

2 mm/min with a 2 kN load cell (Fig. 2b–c).

3-Point Bend Testing of ChitoSand Bilayer: Twelve ChitoSand bilayer samples are prepared using an acrylic mold of 122x38x6 mm following ASTM D790 as above. The mold is placed on top of clamped burlap. Then the burlap is impregnated with chitosan gel with 3 mm thickness, and ChitoSand with flax fiber is applied on top, forming our bilayer. The samples are dried in ambient conditions for 66 h in the mold. An Instron 5564 Tabletop UTM is used with a 2 kN load cell at a loading rate of 2 mm/min and 102 mm-long support spans. The maximum displacement is set to be 6 mm matching the top layer thickness (Fig. 2b–c).

2.3. Internal structure Characterization

Evolution of the Terrene 2.0 microstructure was characterized by

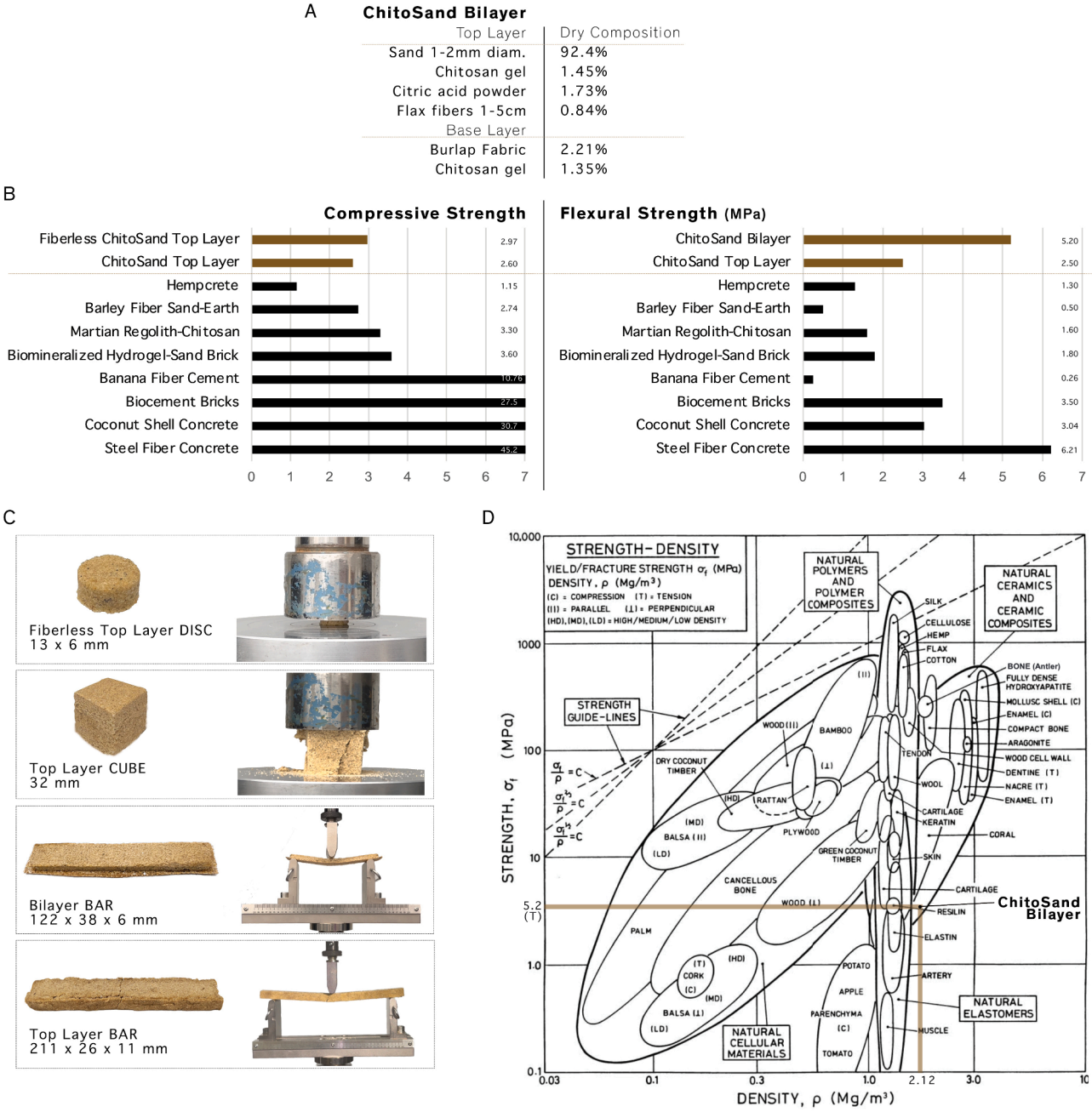

Fig. 2. ChitoSand Bilayer Mechanical Characterization. A) Dry composition of the bilayer system with; predominant quikrete all-purpose sand particles at 1–2 mm diameter, short flax fibers at 1–5 cm length, bound by a water-based mixture of citric acid and chitosan, and laid onto burlap fabric impregnated with chitosan. B) Compressive testing of ChitoSand top layer with (2.60 MPa, σ = 0.15 MPa for 12 samples, 5.77 % deviation) and without flax fibers (2.97 MPa, σ = 0.22 MPa for 12 samples, 7.41 % deviation) shows comparable to other experimental biodegradable sand-based materials [23,24,25,28], and expectedly lower than any cement-based materials [27,29,33]. Flexural testing of ChitoSand top layer with flax fibers (2.50 MPa, σ = 0.41 MPa for 10 samples, 16.4 % deviation) and of ChitoSand bilayer (5.20 MPa, σ = 0.64 MPa for 12 samples, 12.31 % deviation) shows superior to other experimental biodegradable sand-based materials [24,25,28] as well as to natural fiber reinforced cement materials [27,29], and promisingly comparable to steel fiber reinforced concrete [33]. While the inclusion of flax fiber slightly decreases the material's compressive strength, its combination with the burlap layer has a positive effect on flexural strength making it a beneficial addition to ChitoSand. C) Four testing setups are used to determine the ChitoSand bilayer performance in compression and bending regimes and D) the bilayer is comparable in density and strength to weak natural ceramics such as coral and to other more elastic materials like resilin and elastin ().
adapted from [12]

doping the matrix with fluorescent microspheres (fluoromax brand polystyrene microspheres with an average diameter = 2 μm; λex = 542 nm, λem = 612 nm)) under a Confocal Laser Scanning Microscope (Leica Stellaris 5 Model). ChitoSand was spread as a layer (thickness 1 mm) on top of a coverslip to perform confocal microscopy measurements. Images of the first layer of the coverslip were obtained over a span of 5 min at a rate of 0.5 framerates/min, beyond which the microstructure remained unchanged (Fig. 3).

2.4. Structural design

The structure is designed using polyhedral graphic statics (PGS), a geometry-based form-finding technique. In this technique, a specific methodology for generating shell-based cellular (shellular) funicular structures is utilized [31,32]. As displayed in Fig. 4a, in PGS, the equilibrium of a node with four external forces as a form diagram (bottom) can be displayed using a closed convex tetrahedron as a force diagram (top). These two diagrams are reciprocal, meaning that each vertex,

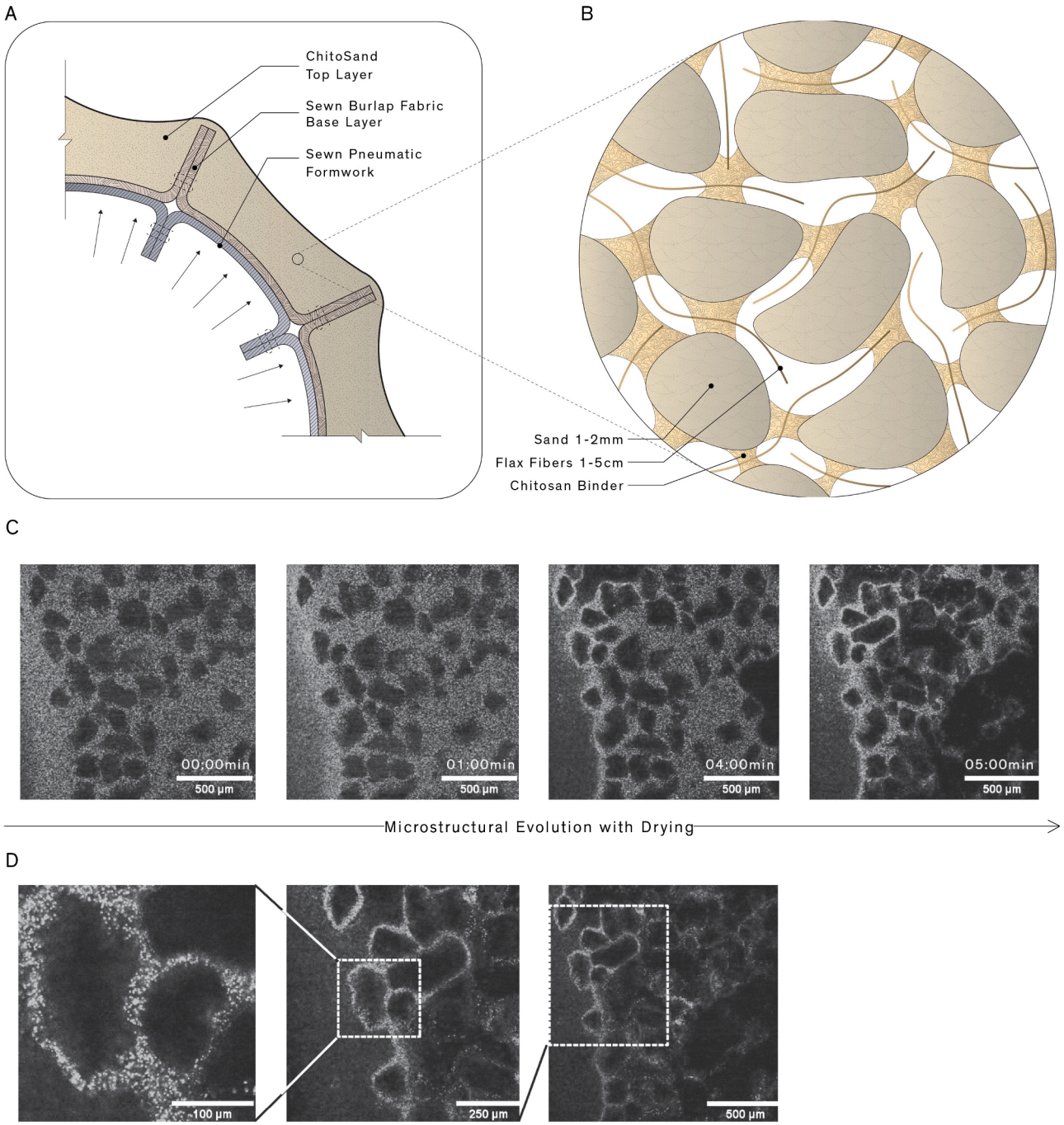

Fig. 3. Terrene 2.0 Internal Structure. A) Construction section drawing of ChitoSand bilayer including; top layer of sand-based compound, base layer of chitosan impregnated burlap fabric with outward finns from sewn polygonal pattern, and supported by pneumatic inflatable formwork fabricated using the same polygonal flat pattern as burlap fabric. B) Drawing of ChitoSand top layer microstructure interactions between sand particles, chitosan binder, and flax fibers. C) Microstructural evolution over a span of 5 mins. At the start of the drying experiment, dye particles (bright domains) occupy the space between the sand particles (dark domains). Over time, as drying proceeds, the bright dye particles in the chitosan binder move towards sand particles forming space-spanning structures. D) Arrangement of dye particles within the chitosan binder demonstrates capillary and pendular bridge formations between the sand particles.

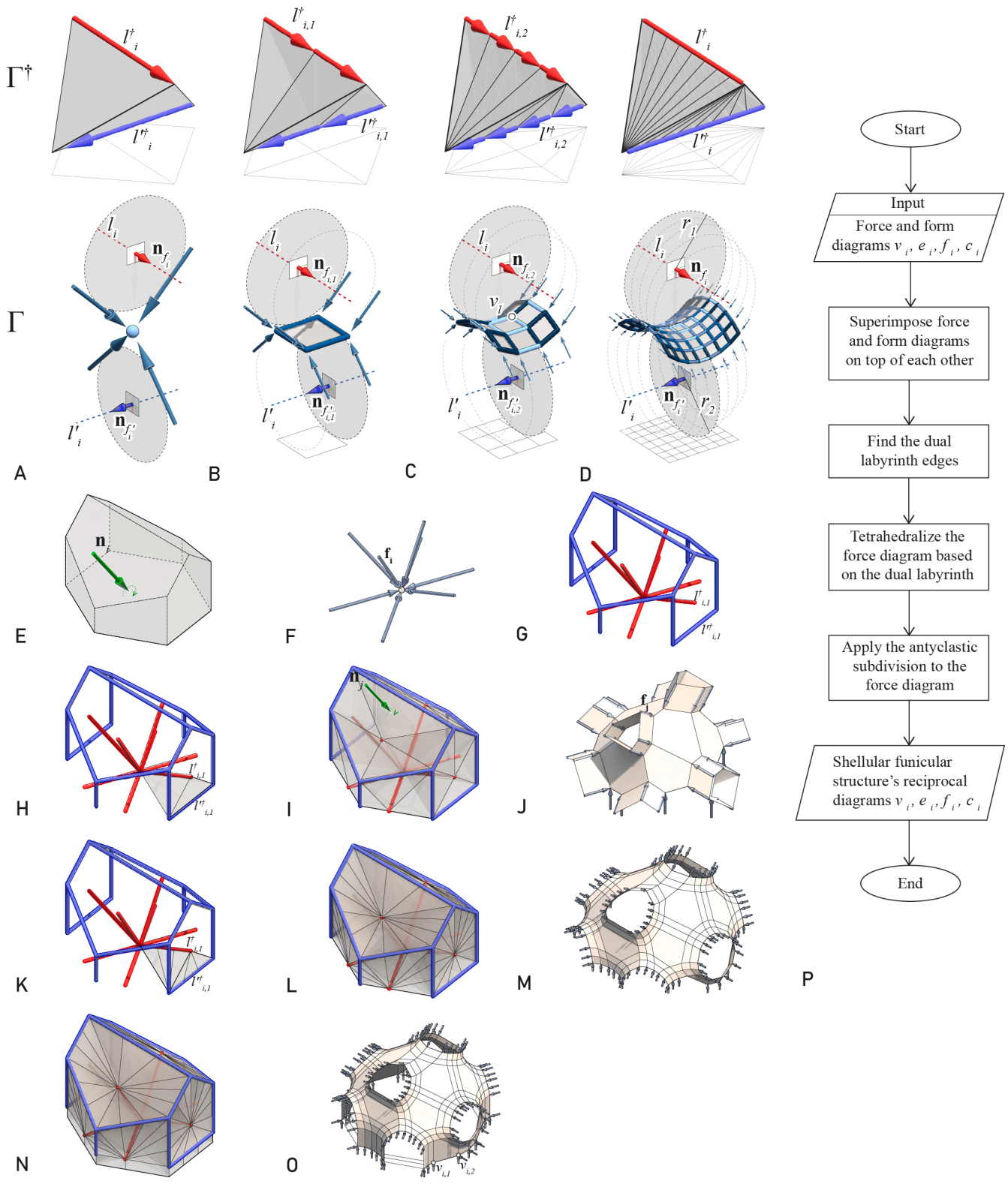

Fig. 4. Form Finding Process: The form finding process starts with the process of designing an anticlastic shell from a node in Polyhedral Graphic statics (A-D), Defining initial force and form diagrams based on loading scenario (E,F), superimposing the diagrams (G), tetrahedralizing the force diagram and applying the anticlastic subdivision resulting in the new shellular form diagram (H-M), extruding the force diagram downwards in order to constrain the supports of the form diagram to the ground (N), and constraining the vertices at the bottom of the structure to the flat ground (O). Lastly, the flowchart related to the form finding process is included as well (P).

edge, face, and cell in the force diagram corresponds to a cell, face, edge, and vertex in the form diagram, respectively. Moreover, the magnitude of the force in each edge in the form diagram is proportional to the area of the corresponding face in the force diagram. Therefore, using this technique, one can design 3d polyhedral structures while having control over the force distribution of the system. Subdividing the tetrahedron as a force diagram results in more complex structures as a form diagram. A specific subdivision, named anticlastic subdivision, can translate a node to a discrete anticlastic surface as a form diagram. Fig. 4b–d displays the process of subdividing a tetrahedron between two skewed edges. These edges, which are named labyrinth graphs, play the role of subdivision axes in the force diagram and curvature axes in the form diagram. According to Fig. 4d, subdividing the force diagram between two axes marked with red and blue colors results in an anticlastic surface as a form diagram with the same axes as curvature axes. Designing a specific labyrinth graph comprising a group of red and blue axes can be considered an initial level for constructing a shellular force diagram. It is important to notice that these labyrinths should be designed in a way that each two reciprocal labyrinths are in a skewed position to each other, enabling the designer to construct a tetrahedron in between.

According to a novel form finding subdivision technique developed by Akbari et al. [32], by superimposing the force and form diagrams of a structure with a certain boundary conditions, one can generate a shellular funicular structure for the specified boundary condition. This process starts with defining the boundary condition. Fig. 4e,f represents the force and form diagrams of a node in equilibrium with nine external loads as the starting configurations. By superimposing the force and form diagrams on top of each other (Fig. 4g) we construct the labyrinth graphs corresponding to our shellular form diagram. This graph comprises two sets of connected edges in specific positions to each other. In this graph, each edge of the red labyrinth set can generate a tetrahedron with specific edges in the blue set. For instance, edge $l^{\dagger}_{i.1}$ is in a skew position with $l'^{\dagger}_{i.1}$, and a tetrahedron can be generated between these two edges (Fig. 4h). This process can be extended to all of the edges that are in skewed positions to each other in order to tetrahedralize the whole force diagram (Fig. 4i). This force diagram corresponds to a form diagram of a two-manifold shell (Fig. 4j). It is important to notice that in this translation to a form diagram, the faces of the form diagram are visualized. To achieve a two-manifold form diagram, in this visualization process, all of the faces in the form diagram corresponding to the labyrinth edges in the force diagram are eliminated. If we apply an anticlastic subdivision to the tetrahedron between two edges $l^{\dagger}_{i.1}$ and $l'^{\dagger}_{i.1}$ (Fig. 4k), and extend this process to all of the labyrinth edges in the force diagram (Fig. 4l), we get a new force diagram corresponding to a shellular funicular form diagram (Fig. 4m). Similar to the previous step, it is worth mentioning that in this form diagram, only the faces are visualized that do not correspond to the labyrinth edges of the force diagram. In the last step, we need to constrain all the vertices at the bottom of the structure to a flat ground. To do this process, we can simply extrude all the faces at the bottom of the force diagram downward (Fig. 4n), resulting in a new form diagram (Fig. 4o) with vertices constrained to the ground (e.g., $v_{i.1}$ and $v_{i.2}$). Fig. 4p illustrates the complete process of form-finding through a flowchart.

In earlier studies, shellular funicular structures were explored as compression-only designs for a particular loading condition [31,32]. In this study, we concentrate on creating shellular funicular structures with

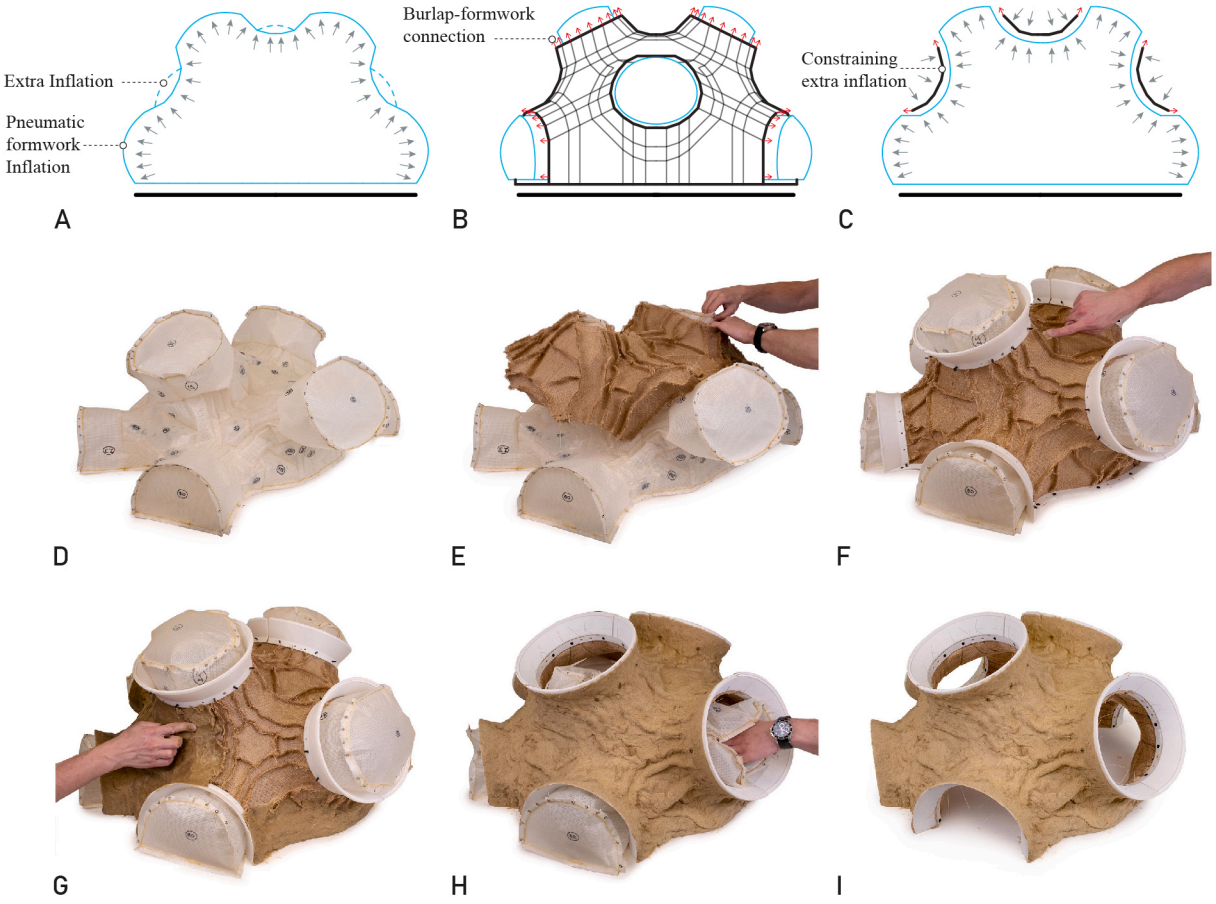

Fig. 5. Form Finding and Fabrication: The model is fabricated on top of a pneumatic formwork and then solidified. Inflating the pneumatic formwork results in the geometry of the designed shell structure (A), but this process may cause extra inflation. Adding a nonstretchable fabric on top of the formwork (B,C) constrains the extra inflation resulting in a precise outcome. **Fabrication Process:** D) pneumatic formwork inflation, E) application of burlap sleeve and PLA frames, F) chitosan gel applied to burlap fabric to form base layer, G) ChitoSand top layer administered to burlap exterior, H) removal of pneumatic formwork, I) completed model.

anticlastic geometry capable of carrying the compression and tension forces. This approach ensures that the proposed material's performance is assessed under both types of forces. Additionally, the technique produces anticlastic patches with flat faces, simplifying the fabrication process by eliminating the need for geometric rationalization.

In the fabrication process, to ensure results in a precise geometry, we start from a pneumatic formwork (Fig. 5a,d), fabricating the shell structure using a stretchable non-stretchable fabric on top of that (Fig. 5b,c,e) and solidifying it using our proposed material (Fig. 5f). Inflating the pneumatic formwork may result in extra inflation, generating errors in the fabrication process. Applying a non-stretchable fabric on top of the pneumatic formwork ensures the precision of the final geometry (Fig. 5b,c,e). Furthermore, after applying the fabric on top of the formwork, a burlap-formwork connections connect the fabric to the formwork, generating a precise geometry comparable to the generated form diagram in the form finding process (Fig. 5b,c).

A finite element analysis is performed to evaluate the structural capacity of this geometry and ensure that the structure is capable of tolerating both tension and compression forces. The geometry's length and width are 60 cm, and the height is around 30 cm. With ChitoSand as the material, this analysis generates a tetrahedral mesh of approximately half a million elements using elastic, perfectly plastic behavior. The structure is simply supported at its base and withstands its gravitational load. According to the analysis, the maximum stress of the structure is around 0.26 MPa, which is less than the maximum compressive strength of the material (i.e., 2.6 MPa). Therefore, the structure can withstand this load and is stable (Fig. 6a,b). Fig. 6c,d represent the Minimum and Maximum Principal Stress, respectively. The Minimum Principal Stress diagram shows that the red colored part of the structure is in tension while the orange colored part is in compression, both with stresses less than maximum compressive/tensile strength of the material. The Maximum Principal Stress diagram represents that the whole structure's stresses in this direction are in compression. Therefore, this structure is under tension and compression stresses and is capable of tolerating its own self-weight.

2.5. Fabrication Steps

Once the chitosan flakes are broken down using acetic acid to a 7 % w/v chitosan mixture, sand, chitosan, flax fibers, and citric acid are mixed using a 2100 W Electric Concrete Mixer. Then, reusable pneumatic formwork is custom-cut from PVC-coated polyester fabric and welded to a shape corresponding to the form-found hybrid geometry. The same pattern is used to sew together burlap fabric patches. For this prototype, oculus rings are 3D-printed from PLA (polylactic acid) filament using a fused deposition filament desktop machine. Pneumatic formwork is inflated with a compressed air pump and connected to the rings using a tensioned cable system. The sewn burlap system impregnated with chitosan resin is then placed on top. Finally, the sand-based mixture is applied, defining the ChitoSand bilayer composite together with the burlap fabric system. Once the bilayer has hardened, the reusable inflatable is removed (Figs. 5, 7, 9).

3. Results: Material performance and system development

We prove below that Terrene 2.0 brings together the design of multiscale biomaterials behavior and efficient structures displaying compression-tension capacity.

3.1. Biomaterial composite design and performance

With a compressive sand matrix as a base, Terrene 2.0 ChitoSand bilayer composite uses renewable resources for the development of a biodegradable material system. To enhance the mechanical properties of the sand matrix, chopped flax fibers are added for tensile strength, citric acid functions as a natural plasticizer, and chitosan acts as a traditional resin binding the mixture's structure within and to a base layer of burlap fabric while it naturally hardens (Fig. 2a, 3a). Based on prior compound development described in [30] a flax-based blend is selected, and mechanical testing results show its potential to build compression-tension anticlastic structures as shown in this work. Compression testing of the ChitoSand top layer with (Fig. 2c-2) and without flax fibers (Fig. 2c-1) shows a strength at break of 2.97 MPa and 2.6 MPa respectively, which is comparable to other experimental biodegradable sand-based materials ranging from 1.15 to 3.3 MPa [23,24,25,28]. The compressive capacity of the ChitoSand top layer is expectedly lower than other naturally augmented cement-based materials (at 10.75 MPa to 45.2 MPa compressive capacity [27,29,33]) which ranges close to traditional concrete (Fig. 3b-left). The flexural capacity of the ChitoSand top layer is 2.5 MPa (Fig. 2c-4) which tested expectedly higher than the top layer bar tests without fiber. What is remarkable is that even if its fiber content is only 0.9 % the bending resistance ranges superior to other fiber-reinforced concrete alternatives such as hempcrete at 1.3 MPa [23], barley fiber sand soils at 0.5 MPa [24], and 5 % banana fiber cements at 0.26 MPa. The flexural performance of the top layer is also expectedly higher than other sand-based experimental materials not reinforced by fiber such as 50:1 regolith-chitosan composites at 1.6 MPa [25], and biomineralized sand-hydrogel blends at 1.8 MPa [28]. The flexural capacity of the entire ChitoSand bilayer (Fig. 2c-3) is at 5.17 MPa, which is superior to other sand-based experimental materials or concretes with sustainable additives such as 10 % coconut shell concrete materials at 3.04 MPa [27], microbial enabled biocements at 3.5 MPa [29] (Fig. 2b-right). More importantly, the ChitoSand bilayer's bending strength is promisingly comparable to 1 % steel fiber reinforced concrete at 6.21 MPa [33] and comparable in density and strength to weak natural ceramics such as coral and to more elastic materials like resilin and elastin [12] (Fig. 2d).

When considering the data deviations of ChitoSand, the compressive strengths exhibit variations ranging from approximately 5.77 % (with fiber) to 7.41 % (fiberless), indicating some degree of variability while remaining within an acceptable range. In contrast, concrete displayed a narrower deviation of 3.88 % in its compressive strength [46], suggesting a more uniform behavior. Notably, other bio-based alternatives such as the biomineralization hydrogel sand brick [28], have a deviation of 9.08 %, and the barley sand earth has a deviation of 7 % [24]. Examining ChitoSand's flexural strength, there is a deviation ranging from 12.31 % (fiberless) to 16.4 % (with fiber), displaying a significant

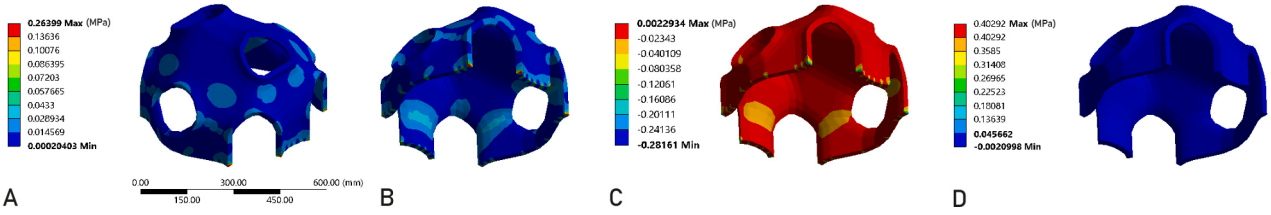

Fig. 6. Mechanical Performance: FEA analysis represents the structural behavior of the geometry under its self-weight including; Equivalent (von Mises) Stress - top view (A), Equivalent (von Mises) Stress - bottom view (B), Minimum Principal Stress - bottom view (C), and Maximum Principal Stress - bottom view (D).

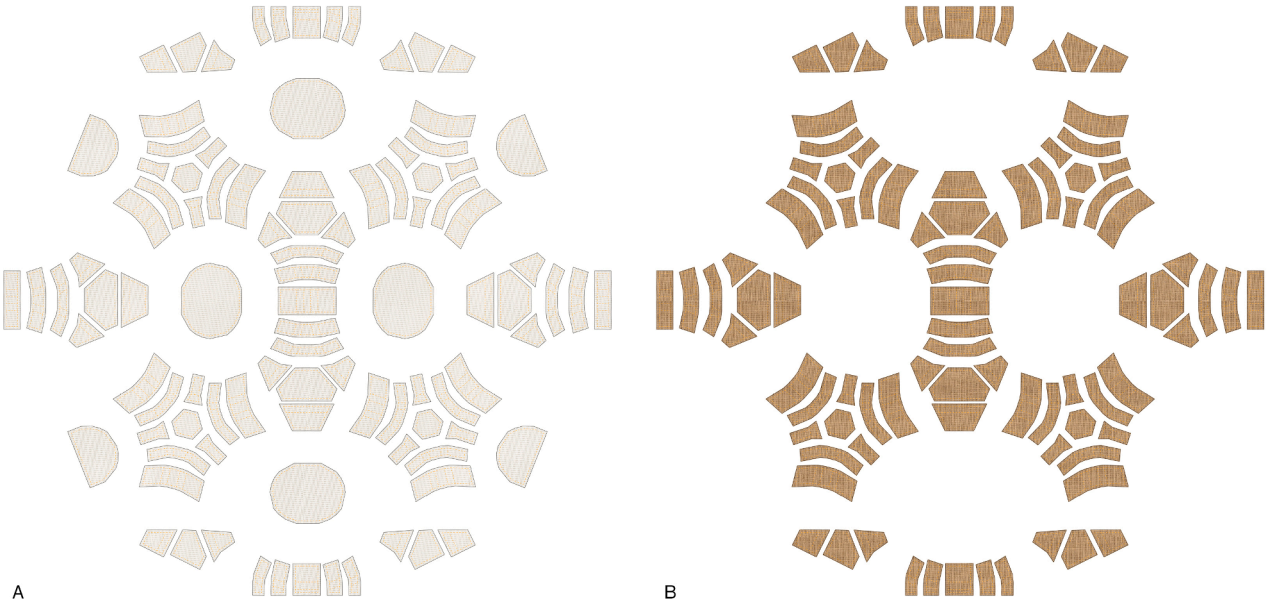

Fig. 7. Fabrication Preparation: TPMS hybrid geometry unrolled into planar surfaces for fabrication: A) pneumatic formwork and B) burlap base layer.

variability in consistency across the different formulations. For comparison, concrete's flexural deviation is only 3.38 % [46], showing a strong consistency between compression and flexural deviations. These deviations provide additional insights into the nuanced mechanical characteristics of ChitoSand, highlighting its potential for diverse applications and areas of improvement.

When observing the compound under the microscope, the microstructure evolves with time as the water evaporates, evidencing the hypothesized internal structure in Fig. 3b. Dye particles acting as tracers are dispersed in the chitosan matrix (Fig. 3c), and their preferential accumulation is observed between the sand grains forming bridging structures between them. These are capillary and pendular bridging structures that bind the sand particles together. The mechanism is similar to post-print curing due to capillary infiltration of nanoparticle binders between granular powders in binder jetting additive manufacturing processes [34,35,36]. When the water in the chitosan binder evaporates, the particles are drawn to form bridges due to capillary pressure (Fig. 3d) strengthening the microstructure. The ChitoSand biomaterial bilayer is effectively designed with multiscale behavior displaying compression-tension capacity induced by (1) strengthened binding by capillary bridges at the microscale, (2) tensile behavior induced by top layer's short flax fibers at the mesoscale, and (3) bending resistance increased by stiffened burlap base layer at the macroscale.

3.2. Design and fabrication of Terrene 2.0 hybrid structure

The construction method consists of five components: (1) pneumatic formwork, (2) tension cables, (3) opening framings, and ChitoSand composite bilayer made of (4) sand-based top layer, and (5) burlap fabric base layer (Fig. 3a). A 1 m2 scaled model to demonstrate this construction method was built. From the planar surfaces resulting from polyhedral graphic statics calculation of the TPMS Hybrid geometry (Fig. 4) (Section 2.4), a reusable pneumatic formwork is fabricated (Fig. 5e). The planar surfaces that infill each of the openings are perpendicularly extended by an additional 10 cm to provide tension support to the burlap fabric network. These planar surfaces are then unrolled flat and offset by 1 cm to provide proper seaming clearance and numerically organized and used to accurately cut out the pneumatic formwork's panels from the lightweight PVC-coated polyester fabric (Fig. 7a). These panels are then sewn together with a zig-zag stitching pattern and sealed with transparent caulking along the interior and exterior of every seam. Grommets are installed along the edge of the extended planar openings and tension wires are attached. Utilizing the same templates from the fabrication of the pneumatic formwork, burlap pieces are cut to specification, but without the inclusion of the opening extensions (Fig. 7b). The burlap pieces are then sewn together using the same zigzag stitch pattern to prevent any seams from splitting under the inflatable's outward pressure. Grommets are installed at the burlap sock edges too. Once this burlap sock is fit over the pneumatic formwork (Fig. 5e), the tension wires are fastened between the grommets from pneumatic formwork to burlap (Fig. 8a). When the system is inflated, these wires pull the structure into tension, providing an accurate base to construct upon and structurally strengthen the system. The PLA base plates are fastened to the foundation, anchoring the burlap fabric along its bottom edge to help prevent uplift from occurring (Fig. 9). The PLA frames are fastened in place to the burlap to provide a clean edge to the openings at the end of construction (Fig. 8b). With the pneumatic formwork inflated to 200 PSI, chitosan gel is applied to the surface of the burlap fabric to saturate and stiffen it, emulating a base layer shell (Fig. 5f). Then the sand mixture is deposited onto the stiffened burlap fabric shell, which enables a solid bond to materialize between the two as they dry in unison (Fig. 5g, Fig. 8c). As the sand-based material continues to be applied, the burlap fins that form along each seam embed themselves to provide additional tensile strength to the system. The total thickness of the applied ChitoSand is 2 cm, allowing for the burlap fins to fully embed themselves within the material. The structure is left to dry in ambient air conditions for 24 h before the tension cables are cut and the pneumatic formwork is deflated and removed (Fig. 5h). The final shellular structure (Fig. 5i, Fig. 9) has supported its own weight without deflection for 12 months and presents a soft interior finish using natural materials for healthy construction (Fig. 10).

4. Discussion: Augmented earthen construction

This research brings new use to renewable resources within the construction industry offering alternative shell materials and methods for reducing our overall carbon footprint. A material-to-shape sustainability-informed design process is achieved through biomaterial blend design and structural form-finding methods.

Fig. 8. Global Fabrication Steps: A) application of burlap sleeve to pneumatic formwork, B) anchoring of PLA frames to burlap, C) ChitoSand administered to burlap exterior.

Fig. 9. Completed model exterior with 10 cm tall figure for scale.

4.1. Advantages of Terrene's materials

Inspired by the methods of earthen construction, Terrene 2.0 looks to improve upon this tradition by providing a more sustainable alternative to single-use formworks and enhancing mechanical properties through the introduction of select pervasive and natural additives. To improve upon the tensile and compressive mechanical properties of a sand base, renewable fibers and textiles, food-grade plasticizers, and biopolymer binders are included to increase tensile capacity, stiffness, and elasticity. These materials offer a natural and renewable solution to earth-based material enhancement rather than the introduction of steel members. The resulting ChitoSand composite acts as a tension–compression material system that can solidify by water evaporation in ambient air conditions. It then minimizes carbon footprint not just within the sourcing of the material, but also in bypassing cement, bricks, or ceramics' gaseous emissions during curing and firing [37,38,39]. Therefore, Terrene 2.0 renders an accessible low-carbon impact construction material. Although ChitoSand testing reveals performance comparable to other sustainable concrete alternatives and interestingly similar to steel fiber reinforced concrete, the material's augmented behavior is gained through carefully designed geometries and construction.

4.2. Topological design intelligence

Typically, the construction of an anticlastic geometry is extremely challenging with conventional mathematical methods [40]. But using the shellular methodology in the context of polyhedral graphic statics,

Fig. 10. Completed model interior with 10 cm tall figure for scale.

one can design and manipulate a shellular funicular structure with anticlastic curvature, while having control over the force path in the structure. One of the main advantages of this technique is designing discrete shellular structures with flat faces which dramatically simplifies the construction process. The designer determines the overall dome-like shape, its apertures, and entry points responding to lighting and occupancy demands, then runs form-finding software (Section 2.4) with specific loading conditions to confirm that the structure and material compositions align with the desired hole distribution. The geometry is constructed through a series of planes and edges that can be simplified by merging the tangential surfaces that still follow the form's flow of forces. This allows for the number of seams to be reduced while maintaining a high resolution in the appearance of the anticlastic geometry, but additional seams can be added to improve the structure's overall strength. These surfaces are then unrolled into a flat pattern for fabrication, making it an easy translation from a complex digital geometry to a constructible physical network. Therefore, the form-finding technique of polyhedral graphic statics is valuable for maximizing structural and material efficiencies and provides a proven approach to translating the digitally developed formal typology to an accurate and tangible physical means of construction.

4.3. Renewable, Reusable, and healthy construction

Our fabrication process uses reusable pneumatic formwork. Typical construction formwork is either constructed out of wood, steel, or aluminum [41,42]. Wooden formwork is currently the most common as it is cheap and customizable, but it is designed for a single use before being discarded [43]. With industry-dominant materials such as concrete requiring a formwork for all its construction applications, a single-use solution produces a lot of excess waste, leading to additional resource depletion and CO2 emissions. While steel and aluminum formworks can be reusable, they are generally heavy, costly, and only applicable to specific geometric typologies, limiting their construction applications [43,10]. Therefore, inflatable formwork could help minimize waste, fabrication costs, and transportation costs during the construction process of low-viscosity materials. To increase the tensile strength of earthen construction, pre- or post-tensioned steel rods are typically introduced into the systems assemblage [44]. However, our burlap fabric base layer contributes a sustainable alternative to providing the surface assembly with a pre-tensioned network. This fabric system is biodegradable and renewable, providing an alternative to using metal tension rods that require a pollutant-producing mining process to gather and manufacture [45]. Additionally, this base layer gives an adequate surface for the ChitoSand to adhere to, enabling the fins of the burlap network to embed themselves within. With the system working cohesively, mechanical strength is increased, expanding the typological possibilities. The fabric finish on the interior of the structure also enables a comforting surface for the livable space and provides the framework for additional customizable surface designs.

5. Outlook: Towards Terrene 3

Terrene 2.0 augments earthen construction and defines new biomaterial composites to form shellular structures with minimal material use for maximum performance. It produces minimum waste through built-in design, material, and fabrication intelligence. In creating a dialogue between each, we produce renewable and reusable architectural systems that reduce the construction industry's overall carbon emissions. Expanding upon the foundations laid by Terrene 1.0 [30], additional material explorations and the refinement of the construction method provide a sustainable and renewable system that has greater mechanical properties and architectural possibilities. Our current research looks toward scaling up the system for Terrene 3.0 to

enclose a full-scale space through the production of a wide-leg arch demonstrator.

CRediT authorship contribution statement

Liam Lasting: Writing – original draft, Methodology, Conceptualization. **Mostafa Akbari:** Writing – review & editing, Methodology, Formal analysis. **Destynn Keuchel:** Writing – review & editing, Writing – original draft, Methodology, Formal analysis. **Na Kyung Lee:** Data curation. **Shravan Pradeep:** Writing – original draft, Visualization, Formal analysis, Data curation. **Shivani Chawla:** Investigation. **Abigail Weinstein:** Investigation. **Masoud Akbarzadeh:** Supervision. **Laia Mogas-Soldevila:** Writing – review & editing, Validation, Supervision, Resources, Project administration, Funding acquisition, Conceptualization.

Declaration of competing interest

The authors declare that they have no known competing financial interests or personal relationships that could have appeared to influence the work reported in this paper.

Data availability

Data will be made available on request.

Acknowledgements

This research was supported by the University of Pennsylvania Research Foundation Grant (URF), and the Johnson & Johnson Foundation Women in STEM2D Scholars Program (USA) to Dr. Laia Mogas-Soldevila. It is also partially funded by the National Science Foundation CAREER AWARD (NSF CAREER-1944691-CMMI, USA), and the National Science Foundation (NSF) Future Eco Manufacturing Research Grant (NSF, FMRG-CMMI 2037097, USA) to Dr. Masoud Akbarzadeh. The authors gratefully acknowledge the use of facilities and instrumentation supported by the Penn LRSM Laboratory for Research on the Structure of Matter (NSF-MRI-1920156-CBET, USA) at the University of Pennsylvania (USA).

References

[1] B. Dillenburger, Additive Construction (2022).
[2] IEA. Global status report for buildings and construction, 2019.
[3] B. Dean, J. Dulac, K. Petrichenko, P. Graham, Towards zeroemission effcient and resilient buildings, Global Status Report (2016).
[4] D. Hoornweg, P. Bhada-Tata, WHAT A WASTE A Global Review of Solid Waste Management. Tech. Rep., The World Bank, 2012.
[5] K. Zhang, P. Chermprayong, F. Xiao, D. Tzoumanikas, B. Dams, S. Kay, B.B. Kocer, A. Burns, L. Orr, C. Choi, et al., Aerial additive manufacturing with multiple autonomous robots, Nature 609 (7928) (2022) 709–717.
[6] M. Mehrpouya, A. Vosooghnia, A. Dehghanghadikolaei, B. Fotovvati, The benefits of additive manufacturing for sustainable design and production, in: Sustainable Manufacturing, 2021, pp. 29–59.
[7] M. Yashar, C. Glasgow, B. Mehlomakulu, J. Ballard, J. Salazar, S. Mauer, S. Covey, Mars dune alpha: A 3d-printed habitat by icon/big for nasa's crew health and performance exploration analog, Earth and Space (2022) 976–984.
[8] A. Szabo, Design and Fabrication of Thin Folded Members with Digital Concrete Processes, PhD Thesis 11 (2020).
[9] J. Head, No nails, no lumber: The bubble houses of Wallace Neff, Chronicle Books, 2011.
[10] A.S. Hanna. Concrete formwork systems, CRC Press, 1998.
[11] M. Popescu, M. Rippmann, T.V. Mele, P. Block, Knitcandela: Chal-Lenging The Construction, Logistics, Waste And Economy Of Concrete-Shell Formworks, Ucl Press, 2020, pp. 194–201.
[12] U.G.K. Wegst, M.F. Ashby, The mechanical efficiency of natural materials, Phil. Mag. 84 (21) (2004) 2167–2186.
[13] Mario Cucinella Architects, TECLA: eco-sustainable housing 3D printed from raw earth, 2020.
[14] L. Mogas-Soldevila, J. Duro, M. Kayser, D. Lizardo, W. Patrick, S. Sharma, S. Keating, J. Klein, C. Inamura, N. Oxman, Designing the Ocean Pavilion: Biomaterial Templating of Structural, Manufacturing, and Environmental Performance, in: Proceedings of IASS Symposium, 2015, Amsterdam NL.
[15] The Living NY. Hy-Fi: Mycelium Brick Towers, 2014.
[16] M.L. Lokko, R. Michael Rowell, A. Dyson, A. Rempel. Development of Affordable Building Materials Using Agricultural Waste By-Products and Emerging Pith, Soy and Mycelium Biobinders, in: 32nd International Conference on Passive and Low Energy Architecture Proceedings, Los Angeles, 2016, pp. 881–887.
[17] J. Lohmann, The Department of Seeweed. PhD thesis, 2017.
[18] L. Mogas-Soldevila, Low Energy Adaptive Biological Material Skins from Nature to Buildings, in: Advanced Materials in Smart Building Skins for Sustainability, 2023, pp. 59–72, ch. 2.
[19] E. Kapoggiani, Geotechnical structures in the ancient' world. the case of the ziggurat of Ur in Mesopotamia, in: Proceedings of the12th International Conference on Structural Analysis of Historical Constructions SAHC, 2020.
[20] B.V. Reddy, Earthen materials and earthen structures, in: Compressed Earth Block & Rammed Earth Structures, 2022, pp. 3–55.
[21] A.M. Neville, et al., Properties of Concrete, 4, Longman London, 1995.
[22] G.E. Troxell, H.E. Davis, J.W. Kelly, Composition and properties of concrete, 1968.
[23] Y. Abdellatef, M.A. Khan, A. Khan, M.I. Alam, M. Kavgic, Mechanical, Thermal, and Moisture Buffering Properties of Novel Insulating Hemp-Lime Composite Building Materials vol. 13 (2020).
[24] A. Koutous, E. Hilali, Reinforcing rammed earth with plant fibers: A case study, Case Stud. Constr. Mater. 14 (2021) e00514.
[25] N. Shiwei, S. Dritsas, J.G. Fernandez, Martian biolith: A bioinspired regolith composite for closed-loop extraterrestrial manufacturing, PLOS ONE 15 (2020) e0238606.
[27] Y. Azunna, F. Aziz, P. Cun, M. Elhibir, Characterization of lightweight cement concrete with partial replacement of coconut shell fine aggregate, SN Applied Sciences 1 (6) (2019) 649.
[28] C.M. Heveran, S.L. Williams, J. Qiu, J. Artier, M.H. Hubler, S.M. Cook, J. C. Cameron, W.V. Srubar, Biomineralization and successive regeneration of engineered living building materials, Matter 2 (2) (2020) 481–494.
[29] G. Dosier, Methods for Making Construction Material Using Enzyme Producing Bacteria, US Patent, 2011.
[30] L. Lasting, I. Isabelle Lee, L. Mogas-Soldevila, M. Akbarzadeh, Terrene 1.0: Innovative, Earth-Based Material for the Construction of Compression-Dominant Shell Structures. Proceedings of the IASS symposium:Innovation Sustainability Legacy, 2022.
[31] M. Akbari, A. Mirabolghasemi, H. Akbarzadeh, M. Akbarzadeh, Geometry-based structural form-finding to design architected cellular solids, in: In *Symposium on Computational Fabrication*, 2020, pp. 1–11.
[32] M. Akbari, A. Mirabolghasemi, M. Bolhassani, A. Akbarzadeh, M. Akbarzadeh, Strut-based cellular to shellular funicular polyhedral materials, Adv. Funct. Mater. (2022) 2109725.
[33] R. Olivito, F. Zuccarello, An experimental study on the tensile strength of steel fiber reinforced concrete, Compos. B Eng. 41 (3) (2010) 246–255.
[34] Y. Bai, C.B. Williams, Binder jetting additive manufacturing with a particle-free metal ink as a binder precursor, Materials Design 147 (2018) 146–156.
[35] F. Liravi, M. Vlasea, Powder bed binder jetting additive manufacturing of silicone structures, Addit. Manuf. 21 (2018) 112–124.
[36] A. Mostafaei, A.M. Elliott, J.E. Barnes, F. Li, W. Tan, C.L. Cramer, P. Nandwana, M. Chmielus, Binder jet 3d printing—process parameters, materials, properties, modeling, and challenges, Prog. Mater Sci. 119 (2021) 100707.
[37] B.M. Skinder, A.K. Pandit, A. Sheikh, B. Ganai, Brick kilns: cause of atmospheric pollution, J. Pollut. Eff. Cont. 2 (112) (2014) 3.
[38] M. Muthukannan, A.S.C. Ganesh, The environmental impact caused by the ceramic industries and assessment methodologies, International Journal for Quality Research 13 (2) (2019).
[39] M. Schuhmacher, J.L. Domingo, J. Garreta, Pollutants emitted by a cement plant: health risks for the population living in the neighborhood, Environ. Res. 95 (2) (2004) 198–206.
[40] W. Meeks III, J. Perez, The classical theory of minimal surfaces, Bull. Am. Math. Soc. 48 (3) (2011) 325–407.
[41] R.L. Peurifoy, G.D. Oberlender, Formwork for Concrete Structures (1996).
[42] W. Li, X. Lin, D.W. Bao, Y.M. Xie, A review of formwork systems for modern concrete construction, Structures 38 (2022) 52–63.
[43] V.W. Tam, J.J. Hao, Prefabrication as a mean of minimizing construction waste on site, Int. J. Constr. Manag. 14 (2) (2014) 113–121.
[44] Q.-B. Bui, T.-T. Bui, R. El-Nabouch, D.-K. Thai, Vertical rods as a seismic reinforcement technique for rammed earth walls: an assessment, Advances in Civil Engineering (2019).
[45] H. Ferreira, M.G.P. Leite, A life cycle assessment study of iron ore mining, J. Clean. Prod. 108 (2015) 1081–1091.
[46] A. Grinys, H. Sivilevičius, M. Daukšys, Tyre rubber additive effect on concrete mixture strength, J. Civ. Eng. Manag. 18 (3) (2012) 393–401.